Research Article | Vol. 25, No. 19 | 18 Sep 2017 | OPTICS EXPRESS 22750
Optics EXPRESS

Spatially localized wavelength-selective absorption in morphology-modulated semiconductor nanowires

JIN SIK CHOI,[1] KYOUNG-HO KIM,[2] AND YOU-SHIN NO[1,3,*]

[1]Department of Physics, Konkuk University, Seoul 05029, South Korea
[2]Department of Chemistry, University of North Carolina at Chapel Hill, Chapel Hill, North Carolina 27599-3290, USA
[3]Department of Chemistry and Chemical Biology, Harvard University, Cambridge, Massachusetts 02138, USA
[*]ysno@konkuk.ac.kr

Abstract: In this study, we proposed morphology-modulated Si nanowires (NWs) with a hexagonal cross-section and numerically investigated their resonant optical absorption and scattering properties. The calculated absorption and scattering efficiency spectra of the NWs exhibited optical resonances that could be controlled by tuning the aspect ratio (AR) of the NW cross-sectional shapes. The spectra also revealed interesting spectral behaviors including resonant peak shifts in the absorption spectrum and asymmetric line shapes in the scattering spectrum. To achieve spatially confined and wavelength-selective light absorption, we periodically modulated the geometry of the diameter in a single NW by combining two different ARs; we call these "diameter-modulated NWs." We designed various diameter-modulated NWs with short and long pitch sizes, and we observed unique and interesting features in the optical resonance and corresponding light absorption spectra such as grating modes and three-dimensional cavity modes. The proposed diameter-modulated NWs can be promising building blocks for the nanoscale localized light absorption and detection in compact nanophotonic integrated circuits.

OCIS codes: (050.6624) Subwavelength structures; (230.5160) Photodetectors; (140.4780) Optical resonators; (040.5350) Photovoltaic; (050.1755) Computational electromagnetic methods.

References and links

1. C. M. Lieber, "Semiconductor nanowires: A platform for nanoscience and nanotechnology," MRS Bull. **36**(12), 1052–1063 (2011).
2. W. Zhou, X. Dai, and C. M. Lieber, "Advances in nanowire bioelectronics," Rep. Prog. Phys. **80**(1), 016701 (2017).
3. R. Agarwal and C. M. Lieber, "Semiconductor nanowires: optics and optoelectronics," Appl. Phys., A Mater. Sci. Process. **85**(3), 209–215 (2006).
4. F. Qian, Y. Li, S. Gradecak, H.-G. Park, Y. Dong, Y. Ding, Z. L. Wang, and C. M. Lieber, "Multi-quantum-well nanowire heterostructures for wavelength-controlled lasers," Nat. Mater. **7**(9), 701–706 (2008).
5. T. J. Kempa and C. M. Lieber, "Semiconductor nanowire solar cells: synthetic advances and tunable properties," Pure Appl. Chem. **86**(1), 13–26 (2014).
6. J. Yao, H. Yan, S. Das, J. F. Klemic, J. C. Ellenbogen, and C. M. Lieber, "Nanowire nanocomputer as a finite-state machine," Proc. Natl. Acad. Sci. U.S.A. **111**(7), 2431–2435 (2014).
7. W. Shim, J. Yao, and C. M. Lieber, "Programmable resistive-switch nanowire transistor logic circuits," Nano Lett. **14**(9), 5430–5436 (2014).
8. B. Tian, T. Cohen-Karni, Q. Qing, X. Duan, P. Xie, and C. M. Lieber, "Three-dimensional, flexible nanoscale field-effect transistors as localized bioprobes," Science **329**(5993), 830–834 (2010).
9. Z. Jiang, Q. Qing, P. Xie, R. Gao, and C. M. Lieber, "Kinked p-n junction nanowire probes for high spatial resolution sensing and intracellular recording," Nano Lett. **12**(3), 1711–1716 (2012).
10. L. Xu, Z. Jiang, Q. Qing, L. Mai, Q. Zhang, and C. M. Lieber, "Design and synthesis of diverse functional kinked nanowire structures for nanoelectronic bioprobes," Nano Lett. **13**(2), 746–751 (2013).
11. Y.-S. No, R. Gao, M. N. Mankin, R. W. Day, H.-G. Park, and C. M. Lieber, "Encoding active device elements at nanowire tips," Nano Lett. **16**(7), 4713–4719 (2016).
12. M. L. Brongersma, Y. Cui, and S. Fan, "Light management for photovoltaics using high-index nanostructures," Nat. Mater. **13**(5), 451–460 (2014).

#303263 https://doi.org/10.1364/OE.25.022750
Journal © 2017 Received 25 Jul 2017; revised 4 Sep 2017; accepted 5 Sep 2017; published 8 Sep 2017

Optics EXPRESS

13. T. J. Kempa, J. F. Cahoon, S.-K. Kim, R. W. Day, D. C. Bell, H.-G. Park, and C. M. Lieber, "Coaxial multishell nanowires with high-quality electronic interfaces and tunable optical cavities for ultrathin photovoltaics," Proc. Natl. Acad. Sci. U.S.A. **109**(5), 1407–1412 (2012).
14. S.-K. Kim, X. Zhang, D. J. Hill, K.-D. Song, J.-S. Park, H.-G. Park, and J. F. Cahoon, "Doubling Absorption in Nanowire Solar Cells with Dielectric Shell Optical Antennas," Nano Lett. **15**(1), 753–758 (2015).
15. L. Cao, J. S. White, J.-S. Park, J. A. Schuller, B. M. Clemens, and M. L. Brongersma, "Engineering light absorption in semiconductor nanowire devices," Nat. Mater. **8**(8), 643–647 (2009).
16. L. Cao, P. Fan, A. P. Vasudev, J. S. White, Z. Yu, W. Cai, J. A. Schuller, S. Fan, and M. L. Brongersma, "Semiconductor nanowire optical antenna solar absorbers," Nano Lett. **10**(2), 439–445 (2010).
17. L. Cao, P. Fan, E. S. Barnard, A. M. Brown, and M. L. Brongersma, "Tuning the color of silicon nanostructures," Nano Lett. **10**(7), 2649–2654 (2010).
18. R. W. Day, M. N. Mankin, R. Gao, Y.-S. No, S.-K. Kim, D. C. Bell, H.-G. Park, and C. M. Lieber, "Plateau-Rayleigh crystal growth of periodic shells on one-dimensional substrates," Nat. Nanotechnol. **10**(4), 345–352 (2015).
19. R. W. Day, M. N. Mankin, and C. M. Lieber, "Plateau-Rayleigh crystal growth of nanowire heterostructures: strain-modified surface chemistry and morphological control in one, two, and three dimensions," Nano Lett. **16**(4), 2830–2836 (2016).
20. J. D. Christesen, C. W. Pinion, E. M. Grumstrup, J. M. Papanikolas, and J. F. Cahoon, "Synthetically encoding 10 nm morphology in silicon nanowires," Nano Lett. **13**(12), 6281–6286 (2013).
21. S. Kim, D. J. Hill, C. W. Pinion, J. D. Christesen, J. R. McBride, and J. F. Cahoon, "Desiging morphology in eptitaxial silicon nanowires: the role of gold, surface chemistry, and phosphorus doping," ACS Nano **11**(5), 4453–4462 (2017).
22. B. Luk'yanchuk, N. I. Zheludev, S. A. Maier, N. J. Halas, P. Nordlander, H. Giessen, and C. T. Chong, "The Fano resonance in plasmonic nanostructures and metamaterials," Nat. Mater. **9**(9), 707–715 (2010).
23. P. Fan, Z. Yu, S. Fan, and M. L. Brongersma, "Optical Fano resonance of an individual semiconductor nanostructure," Nat. Mater. **13**(5), 471–475 (2014).
24. H.-C. Lee, J.-Y. Na, Y.-J. Moon, J.-S. Park, H.-S. Ee, H.-G. Park, and S.-K. Kim, "Three-dimensional grating nanowires for enhanced light trapping," Opt. Lett. **41**(7), 1578–1581 (2016).

1. Introduction

Semiconductor nanowires (NWs), a versatile class of nanomaterial, have expedited the development of a diverse range of devices for nanoelectronics, biochemical sensing, photonics, and energy science [1–5]. They serve a variety of functions that benefit from synthetically controlled morphologies in conjunction with tunable electrical and optical properties [6–11]. For example, a nanoelectronic finite-state machine developed by programmable NW transistor nodes realized a complete two-bit logic flow and clocked control state registration as well as two-bit full adder programmable circuits [6]. Localized and tunable three-dimensional (3D) recordings of intracellular potentials were demonstrated for the first time by kinked Si NWs with synthetically integrated nanoscale field effect transistors [8]. For photovoltaic (PV) NW devices, the controlled morphologies and corresponding optical responses play even more dominant roles because the high refractive index of NWs permits a series of resonant optical modes that enable strong photon confinement [5,12–17]. Thus, the energy conversion efficiency of individual NW PV devices can be significantly enhanced by the tunable light absorption properties that critically depend on the geometry and size of the NWs [13–16]. Therefore, obtaining the desired light absorption properties of single NWs with given morphologies is a prerequisite for optimized PV devices.

Recently, a unique method of nanoscale crystal growth, called Plateau–Rayleigh (P–R) crystal growth, further expanded the ability to control the morphology of NWs [18,19]. P–R crystal growth allows for the successful periodic modulation of diameter in single core–shell NWs. The modulation includes the size and aspect ratio (AR) of the cross-section as well as the modulation pitch along the NW axis. In addition, the nanoscale synthetic encoding of various nanostructures on single NWs, including nanorods, bowties, tapers, and gratings, has successfully been demonstrated by the accurate control of doping and chemical etching [20,21]. These successful demonstrations of morphology modulations have motivated researchers to explore the potential for efficient and functional light absorption in PVs and other photonic applications. In this work, we systematically studied the light absorption and scattering properties of various high-AR uniform NWs and diameter-modulated NWs with

Optics EXPRESS

different pitch sizes. Our numerical investigations reveal interesting spectral features of the resonance in the absorption and scattering efficiency spectra. In addition, we propose key design rules for diameter-modulated NWs to achieve spatially confined and wavelength-selective light absorption within single NWs.

2. Results and discussion

Figure 1(a) shows a schematic of normal and high-AR NWs. The normal NW (left, Fig. 1(a)) has a regular hexagonal cross-section, while the high-AR NW (middle, Fig. 1(a)) has a hexagonal cross-section but elongated in one direction. Here, the AR is defined as the ratio of the width (W) and height (H) of the NW (right inset, Fig. 1(a)). To investigate the fundamental optical properties of the NWs, we varied the AR from 1 to 6 with a fixed height of 100 nm and calculated the total absorption efficiency (Q_{abs}) and total scattering efficiency (Q_{sca}) spectra using a finite-difference time-domain (FDTD) simulation. In the simulation, the incident plane wave with transverse-electric (TE, with the electric field normal to the NW axis) polarization was top-illuminated on the free-standing NW. Periodic boundary conditions were applied along the NW axis and perfectly matched layers were introduced at the other boundaries. A spatial resolution of 5 nm was used. The absorption and scattering efficiencies are defined as the absorption and scattering cross-sections normalized to the geometrical cross-section of the NW [18].

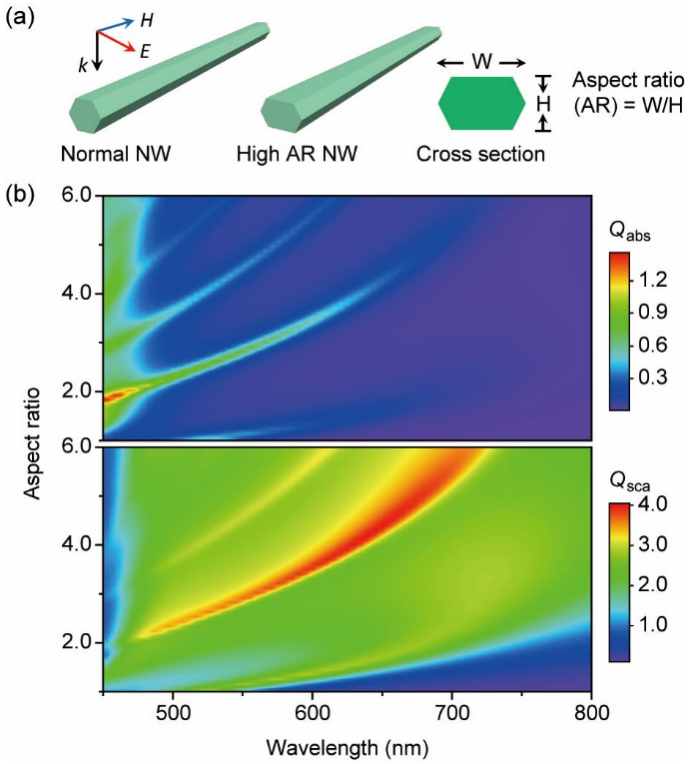

Fig. 1. (a) Schematic illustration of simulation geometry for normal (left) and high-AR NWs (middle) under TE-polarized incident illumination. Right inset: Cross-sectional shape of a NW and the definition of AR. (b) Two-dimensional color maps of the calculated total absorption (top, Q_{abs}) and total scattering (bottom, Q_{sca}) efficiencies of the NWs as functions of wavelength and cross-sectional AR for TE-polarized incident illumination. In the calculations, the height (H) of the NWs was fixed at 100 nm and the AR was varied from 1 to 6 by changing the width (W) of the NWs.

Optics EXPRESS

From the two-dimensional (2D) color maps of the total absorption (top) and scattering (bottom) efficiency spectra in Fig. 1(b), we observe several distinct high-intensity peaks, which red-shift as the AR of the NW increases. A direct comparison between the two color plots reveals the spectral correspondence of these high-intensity peaks, which originates from the optical resonances supported by the NWs. The light absorption in a semiconductor Si NW with a high refractive index can be significantly enhanced when the incident light wavelength is matched to one of the resonant optical modes of the NW [13–16]. At these resonances, light is also strongly scattered by the NW because some of the trapped electromagnetic energy in the resonant optical modes is coupled to the free space radiation modes and is returned to the far-field [17]. In addition, the resonant modes of the NW are easily tuned as the size and geometry of the NW vary, which explains the shift in resonant wavelength with varying AR.

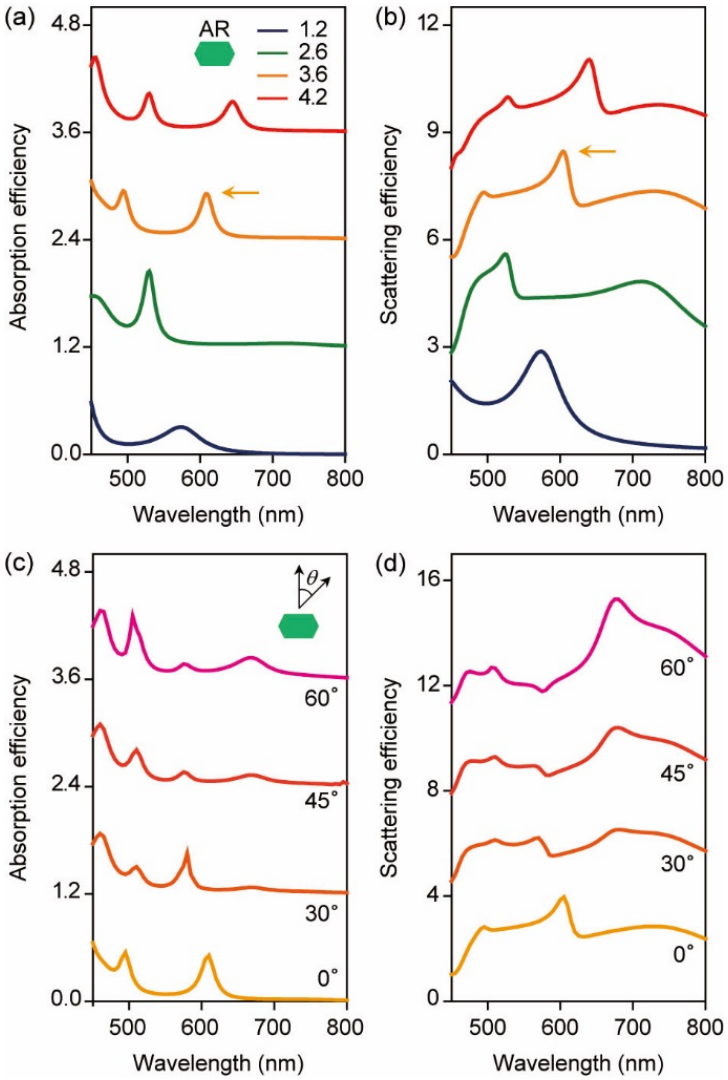

Fig. 2. (a) Calculated absorption efficiency and (b) scattering efficiency spectra of NWs with various ARs of 1.2 (dark blue), 2.6 (green), 3.6 (yellow), and 4.2 (red) under TE-polarized incident illumination. For all calculations, the height of the NW was fixed at 100 nm. (c)–(d) Incident angle-dependent absorption (c) and scattering efficiencies (d) of the NW with AR of 3.6 (yellow arrow in (a) and (b)). Inset in (c) shows the angle of the incident light. Angles of 0°, 30°, 45°, and 60° with respect to the normal incident were simulated.

Optics EXPRESS

In Fig. 2, we selected four representative Si NWs with different ARs and investigated their absorption and scattering spectral behaviors. We calculated the absorption (Fig. 2(a)) and scattering efficiency spectra (Fig. 2(b)) for the NWs with ARs of 1.2 (navy), 2.6 (green), 3.6 (yellow), and 4.2 (red). As expected, a clear red-shift in resonant absorption peak is observed as the AR increases. For example, the absorption peak at 530 nm for the AR of 2.6 shifts to 608 and 644 nm for ARs of 3.6 and 4.2, respectively. In addition, the calculated scattering efficiency spectra exhibit similar resonance behaviors as the NW AR increases. Furthermore, we investigated incident angle-dependent light absorption (Fig. 2(c)) and scattering (Fig. 2(d)) for the NW with high AR of 3.6 (yellow markers in Figs. 2(a) and 2(b)). The angles of 30°, 45°, and 60° with respect to the normal incident were simulated. Calculated absorption and scattering efficiencies with various incident angles exhibited noticeable spectral variations in both line-shape and intensity because the high AR NW breaks the angular symmetry.

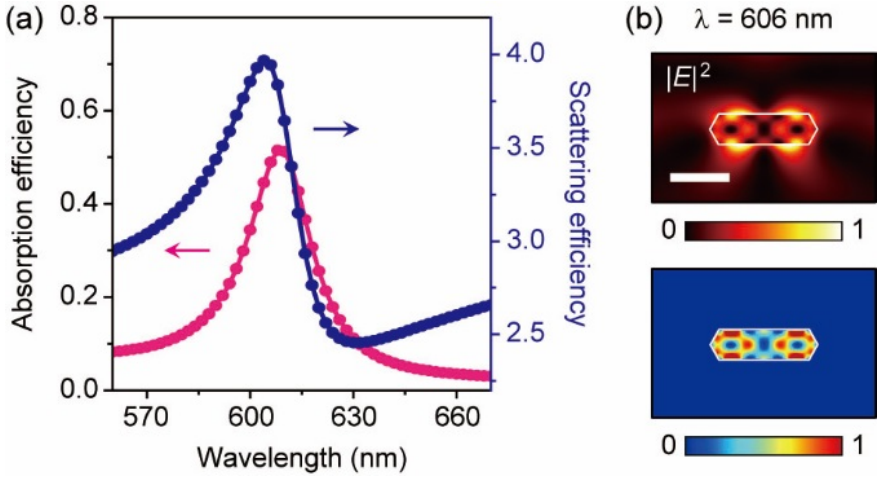

Fig. 3. (a) Co-plot of absorption efficiency (pink) and scattering efficiency (navy) spectra from the NW with AR of 3.6 (arrows in Fig. 2(a) and 2(b)) near the resonant wavelength of 606 nm. (b) Calculated electric field intensity (top) and absorption profiles (bottom) of the NW used in (a) at the resonant wavelength of 606 nm. Both profiles are normalized with respect to their maximum values. The scale bar is 200 nm.

We also note that asymmetric resonant scattering peaks are observed in the NWs with high AR (i.e., AR = 2.6, 3.6, 4.2), while a relatively symmetric line shape of the resonant scattering peak is observed in the NW with an AR of 1.2. Figure 3(a) shows a co-plot of the absorption (pink) and scattering efficiency spectra (navy) near the resonant frequency from the NW with an AR of 3.6 (yellow arrows in Figs. 2(a)–2(b)). They reveal that the resonant scattering peak appears close to, but not exactly at its absorption resonance. The asymmetric line shapes in the light scattering spectra are the consequence of Fano resonance, which results from the interference between resonant and non-resonant scattering pathways [22,23]. The resonant scattering process involves the rapidly varying amplitude and phase near the resonant frequency, whereas the non-resonant scattering process preserves the amplitude and phase with negligible variation. Therefore, the resulting interference gives rise to not only the asymmetric Fano line shape but also the total scattering peak and dip that are slightly offset from the resonant frequency [23]. In Fig. 3(b), we observe the electric field intensity (top) and absorption (bottom) profiles at the resonant wavelength of 606 nm in Fig. 3(a). The distribution of high intensities inside the NW matches the intensity maxima of the absorption profile.

Optics EXPRESS

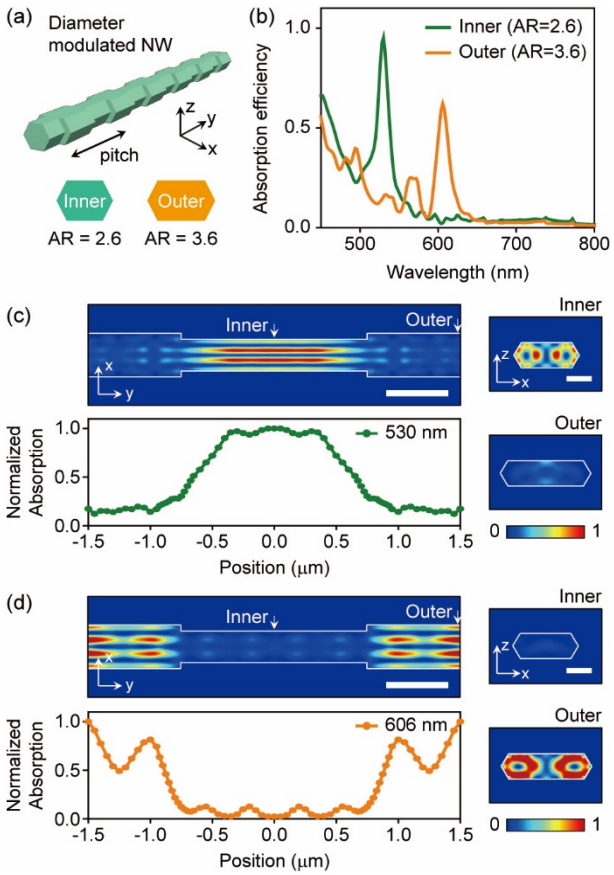

Fig. 4. Spatially localized wavelength-selective light absorption in a diameter-modulated NW. (a) Schematic illustration of the diameter-modulated NW. Two different cross-sectional morphologies (inner and outer) were periodically (pitch) placed along the NW axis. Inset: inner (green) and outer (yellow) cross-sections with the same height but different ARs. (b) Calculated absorption efficiency spectra from the inner (green, AR = 2.6) and outer (yellow, AR = 3.6) segments of the periodically modulated NW. The height and pitch of the NW were 100 nm and 3 μm, respectively. (c)–(d) Calculated absorption profile (left, top) and normalized absorption efficiency (left, bottom) along the NW axis at the wavelengths of (c) 530 and (d) 606 nm. The scale bars are 500 nm. Cross-sectional absorption profiles of inner (right, top) and outer (right, bottom) segments at the wavelengths of (c) 530 and (d) 606 nm. The scale bars are 100 nm.

We explored the ability to tune the optical resonances of high-AR NWs and designed a new NW that experiences a periodic modulation of diameter along the NW axis. Figure 4(a) shows a schematic of this diameter-modulated NW consisting of two different ARs that are alternately placed along the NW axis (*y*-axis) with a given periodicity (pitch). We chose ARs of 2.6 and 3.6 with a fixed height of 100 nm and call the small and large ARs the "inner" (green hexagon) and "outer" (yellow hexagon) segments of the NW, respectively. To investigate the optical properties, we performed full-wave 3D FDTD simulations and calculated the absorption efficiency of the diameter-modulated NW with a long pitch size of 3 μm. Figure 4(b) presents two absorption efficiency spectra from the inner (green solid line) and outer (yellow solid line) segments of the NW. Interestingly, similar spectral behaviors of the inner and outer segments to those from the uniform NWs with the same ARs are observed: the resonant absorption peaks at 530 (inner) and 606 nm (outer) agree with those in the uniform NWs with the same diameters and ARs. There are small additional peaks at 534 and 566 nm from the outer segment that are not found for the uniform NW. We attribute these

Optics EXPRESS

peaks to wave reflections from the boundaries between the inner and outer segments in the diameter-modulated NW. The absorption profiles at the resonant wavelengths enabled further investigation of the resonant absorption properties in the diameter-modulated NW. In Fig. 4(c), we obtained the spatial distribution of light absorption along the NW axis (top, left) at 530 nm, in which resonant absorption occurs for the inner segment. These spectra clearly visualize the strong light absorption only in the inner segment and almost negligible absorption in the outer segment. It is also supported by the cross-sectional absorption profiles of the inner (top right) and outer segments (bottom right) as well as the absorption distribution as a function of position (bottom left). The ratio of absorption in the middle of the inner segment to the outer segment (white arrows; top left) is ~8.2. In contrast, the reverse situation occurs at 606 nm, in which resonant absorption occurs for the outer segment (Fig. 4(d)). From the absorption profiles, we observe the strong light absorption in the outer segment and negligible absorption in the inner segment. Again, a significant difference in absorption of the inner and outer segment (ratio ~0.02) is observed. Taken together, the diameter-modulated NW with the desired cross-sectional ARs enables spatially localized and wavelength-selective light absorption within a single NW, which has been very challenging in conventional uniform NWs.

The diameter-modulated NW exhibits more interesting features when the size of the pitch is reduced to about a few hundred nanometers, comparable to the wavelength of the incident light. In Fig. 5(a), we reduced the pitch of the NW used in Fig. 4 to 440 nm and calculated the total absorption efficiency spectrum (black solid line). Other structural parameters such as the height and AR of the inner/outer segments of the NW were kept identical to those of the NW of Fig. 4. We also calculated the absorption efficiency spectra of a uniform NW with an AR of 3.6 (yellow dotted line) and bulk Si film with a thickness of 100 nm (gray dotted line). Compared with the uniform NW, we observe an overall increase in light absorption in the visible spectral range from 450 to 700 nm. We also observe a slight blue-shift of the resonant peak (e.g., yellow marker in Fig. 5(a)) due to the fast modulation by reduced pitch, which allows for the resonant modes to experience the boundaries between inner and outer diameter more frequently. In particular, we observe a very sharp and strong absorption peak with an efficiency close to unity (~0.94) at 910 nm where the light absorption from the uniform NW and thin film is negligible [18,24]. This pronounced absorption peak originates from a different resonance mechanism compared to the other resonant peaks. The absorption peaks of conventional uniform NWs stem from the resonant optical modes that form in the 2D cross-section of the NWs. However, with the short pitch size of about a few hundred nanometers, the rapid modulation of diameter along the NW serves as efficient optical gratings that couple some of the top-illuminated incident waves to a transversely propagating waveguide mode through the NW (bottom, Fig. 5(b)) [24]. As a result, this waveguide mode appears when the incident light wavelength matches the grating conditions. Consequently, this guided mode in the near-infrared (IR) regime can easily be tuned by varying the pitch size. In Fig. 5(c), we systematically changed the pitch size from 360 to 480 nm with a step size of 40 nm and calculated the absorption efficiency spectra ranging from 750 to 1000 nm. We observe a clear red-shift in the high-intensity absorption peaks from the waveguide modes as the pitch size increases. For practical applications, we introduced SiO_2 substrate and performed the same simulations. The results show the red-shift of the absorption peaks with slightly reduced intensities. The observed features of the waveguide modes allow unique and powerful controllability of the light absorption in the near-IR regime.

Optics EXPRESS

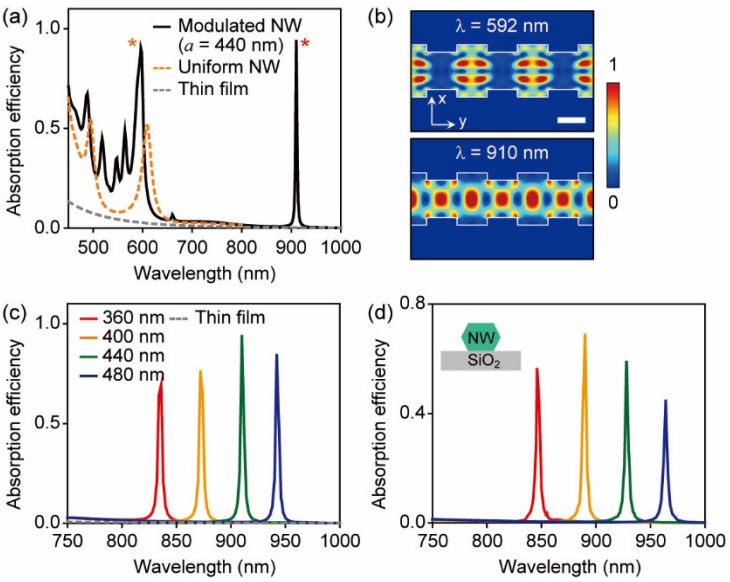

Fig. 5. Wavelength-tunable and enhanced light absorption of waveguide modes in the diameter-modulated NWs with short pitch sizes. (a) Comparison of calculated absorption efficiency spectra of diameter-modulated NW (black line) with a short pitch (a = 440 nm), uniform NW with an AR of 3.6 (yellow dotted line), and thin film (gray dotted line). The height of the modulated and uniform NWs and thickness of the thin film were 100 nm. The ARs of the inner and outer segments of the diameter-modulated NW were identical to those used in Fig. 3. (b) Absorption profiles of the diameter-modulated NW at the wavelengths of 592 (top) and 910 nm (bottom). The scale bar is 200 nm. (c) Wavelength-tunable and enhanced absorption efficiency spectra from waveguide modes in the modulated NWs with various pitch sizes of 360 (red), 400 (yellow), 440 (green), and 480 nm (dark blue). The absorption efficiency spectrum (gray dotted line) of the thin film in (a) was co-plotted for comparison. (d) Absorption efficiency spectra from the same waveguide modes in the NWs on SiO_2 substrate (inset).

Finally, we designed an interesting extreme diameter-modulated NW to further examine the spatial confinement of light absorption. In Fig. 6, we introduced a NW with an ultrathin inner diameter with a height of 30 nm and AR of 1.1 and outer diameters with a height of 100 nm and ARs of 2.6 (Fig. 6(a)) and 3.6 (Fig. 6(c)). The pitch size was fixed at 440 nm for both cases. In Fig. 6(a), we separately calculated the light absorption efficiency spectra from the inner (gray line) and outer segments (red line). Negligible light absorption is found in the inner segment as the reduced cross-section allows no optical modes to be excited. In contrast, a noticeable increase in light absorption at short wavelengths (<550 nm) is observed in the outer segment. Furthermore, we observe a new absorption peak at 664 nm (red arrow, Fig. 6(a)) that is not found in the uniform NW with the same diameter. In addition, with the ultrathin inner diameter much smaller than the incident wavelengths, the outer segment becomes optically isolated from the adjacent inner segments and acts as a 3D cavity that supports the resonant optical cavity modes (top and side views, Fig. 6(b)). Therefore, the absorption peak at 664 nm is distinguished from the conventional resonant modes formed in the 2D cross-section of the uniform NWs. We tested another outer diameter with an AR of 3.6 and observed similar spectral behaviors, as shown in Fig. 6(c). As the AR of the NW increases, the increased physical volume of the NW leads to a red-shift in all resonant absorption peaks compared with those in Fig. 6(a). We note that the absorption peak at 528 nm (conventional resonant mode, Fig. 6(a)) shifts to 584 nm (yellow arrow, Fig. 6(c)). However, the absorption peak at 664 nm (3D cavity mode, Fig. 6(a)) undergoes a relatively small shift to 682 nm (Fig. 6(c)). In Fig. 6(d), we obtained the absorption intensity profile at 584 nm (yellow arrow, Fig. 6(c)), which qualitatively shows similar intensity distributions

Optics EXPRESS

compared with the previous intensity profiles of the diameter-modulated NWs with different pitch sizes (top left, Fig. 4(d); and top, Fig. 5(b)). Taken together, one can efficiently achieve a complete spatial confinement of light absorption by utilizing a diameter-modulated NW with an ultrathin inner diameter.

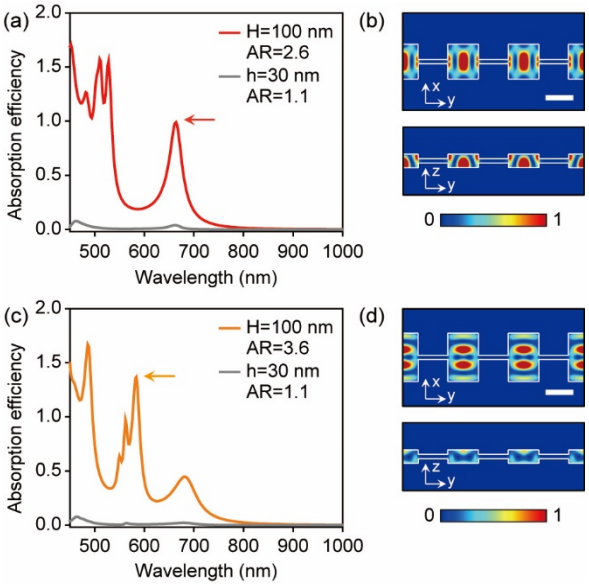

Fig. 6. Spatial confinement of absorption in the diameter-modulated NW with a short pitch and ultrathin inner diameter. (a) Calculated absorption efficiency spectra from the inner (gray) and outer (red) segments of the modulated NW. The pitch size was 440 nm and the height (AR) of the inner and outer segments were set to 30 (1.1) and 100 nm (2.6), respectively. (b) Top (top) and side (bottom) views of the calculated absorption profiles at the resonant wavelength of 664 nm (red arrow in (a)). The scale bar is 200 nm. (c) Calculated absorption efficiency spectra from the inner (gray) and outer (yellow) segments of the modulated NW. The pitch size and height of the NW were identical to those in (a). The ARs of the inner and outer segments were set to 1.1 and 3.6, respectively. (d) Top (top) and side (bottom) views of the calculated absorption profile at the resonant wavelength of 584 nm (yellow arrow in (c)). The scale bar is 200 nm.

3. Conclusions

We investigated the resonant absorption and scattering properties of various high-AR NWs by performing 3D FDTD simulations. By varying the AR of the NWs, the detailed spectral behavior including resonant peak shift and Fano resonance was systematically studied. We designed a diameter-modulated NW consisting of inner and outer diameters with two different ARs of 2.6 and 3.6, respectively. For a long pitch size of 3 μm, the absorption efficiency spectra and intensity profiles from the inner and outer segments exhibited spatially confined and wavelength-selective light absorption within a single diameter-modulated NW. In addition, when the pitch size was reduced to about a few hundred nanometers, we observed a very sharp and strong absorption peak with an efficiency close to unity at a long wavelength of >800 nm, where the diameter modulation gratings act as an efficient coupler and convert the normal incident light into propagating waveguide modes. Furthermore, as an extreme case of modulation, we introduced an ultrathin inner diameter with a height of 30 nm and AR of 1.1 to the NW. From this NW structure, we achieved the complete localization of light absorption in the outer segment by suppressing all optical modes in the inner segment. We believe the proposed diameter-modulated NWs will become important nanoscale components for the localized light absorption and detection in integrated photonic circuits and for exploring novel and promising optical applications.

Optics EXPRESS

Funding

Basic Science Research Program through the National Research Foundation of Korea (NRF) funded by the Ministry of Education (2017R1D1A1B03033668).

Acknowledgment

We thank Professor Charles M. Lieber for helpful discussions during the analysis of the simulation results.